Radiative transfer simulation of dusty stellar systems using Monte Carlo methods

Evangelos Angelou, Andrea Sottoriva

Abstract

Monte Carlo methods for radiative transfer are nowadays well known and widely used in both Astronomy and Physics. The idea behind such techniques is very simple: tt consists on simulating the trajectory of a large number of photons keeping track of their interaction with the travelling media. For a sufficient number of simulated particles such methods have proved to be as accurate as the respective analytical models. However Monte Carlo techniques allow us to simulate systems with an arbitrary distribution of interacting material (e.g. dust).

To understand the meaning of the detailed images produced by modern telescopes, the finest models for radiation transfer become necessary and Monte Carlo methods are a suitable candidate for this task. We have investigated the phenomenon of radiation transfer on dusty stellar systems using Monte Carlo methods. We will discuss several aspects of radiative transfer and we will show the results we obtained. Furthermore we will present a parallelization approach. The simulation is entirely implemented in C++ and using MPI.

1 Introduction

As described before, the concept of Monte Carlo radiation transfer is extremely easy: we generate a new photon from a defined light source (a star) and we let it travel for a certain length, until it interacts with the matter.

The system consists of a star producing photons isotropically and a certain amount of dust between the observer and the light source that influences the trajectories of the emitted photons.

Once the photon is generated, two inportant phenomena may happen along the photon path:

- Scattering

    The trajectory of the particle is deviated according to a certain probability distribution and depending on the type of scattering (electron scattering, dust scattering, ...) and other parameters discussed further.

- Absorbtion

    The photon is absorbed by the matter, the journey is over.

Finally, by projecting all the surviging photons onto the observer's plane, it is possible to generate images.

1.1 History

Monte Carlo methods are known from the beginning of the 20th century, when they were generically called *statistical sampling*. The name *Monte Carlo* refers to their randomness and repetitiveness, characteristics in common with the famous *casino* of Monaco.

Such a fancy name became popular thanks to famous physicists like *Stanislaw Ulam*, *Enrico Fermi*, *John von Neumann* and *Nicholas Metropolis*. The story narrates that Ulam's uncle, a well-known hardcore gambler, would constantly borrow money from friends and relatives because he "just had to go to Monte Carlo". From there the name *Monte Carlo methods* proposed by Ulam[4].

Probably the most famous early use of Monte Carlo techniques was by Enrico Fermi during his studies in Rome on the *moderation of the neutron*. There he was performing Monte Carlo calculations using mainly a small mechanical adding machine. Afterwards, while working in the ENIAC operation in Los Alamos, Fermi persuaded his friend and collaborator Percy King to build an improved and ingenious version of his old adding machine. Such instrument was called *FERMIAC* or Monte Carlo *trolley* (Figure 1) and it was used to determine neutrons collision paths in numerous nuclear systems[4].

Thereafter, Monte Carlo methods played (unfortunately) a central role in the *Manhattan* project and in the successive atomic bombs experiments, when they started to become more and more famous in other fields of science and in business. Monte Carlo techniques have been also important for
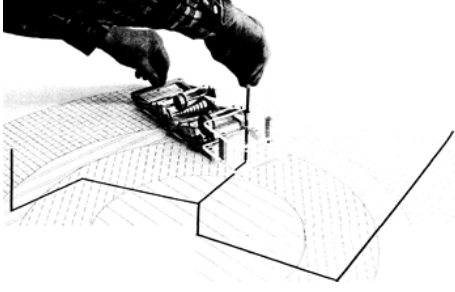
Figure 1. The FERMIAC

the development of better and more efficient random number generators. They led to the creation of the *linear congruential generators*, a necessary alternative to the random number tables used until the '50s.

2 Radiation transfer: theoretical background

We first introduce some basic concepts of radiative transfer, necessary to understand the processes we are modeling.

2.1 Basic concepts

Considering a unit surface dA at an angle θ to its normal, within a solid angle $d\Omega$ and a frequency range $d\nu$ in a time interval dt, the intensity I_ν is defined with respect to the radiant energy dE_ν as:

$$I_\nu = \frac{dE_\nu}{cos\theta \, dA \, dt \, d\nu \, d\Omega} \tag{1}$$

It is measured in $[ergs \, cm^{-2} \, s^{-1} \, Hz^{-1} \, sr^{-1}]$ and denotes the radiation energy (within a certain frequency) crossing a certain area with a certain direction per second. Another important term, the flux F_ν, is the energy that crosses an area dA per unit of time:

$$F_\nu = \int I_\nu cos\theta d\Omega \tag{2}$$

measured in $[ergs \, cm^{-2} \, s^{-1} \, Hz^{-1}]$.

Those two terms play a central role in the process of radiation transfer.

Furthermore, being the cross section σ the likelihood of interaction between the photons and the particles in the media, the energy removed per second per frequency per solid angle from the direction of travel (by either scattering or absorbtion) is:

$$E_r = I_\nu \, \sigma \tag{3}$$

Considering then the cross section and the density n of the material, the differential intensity along a length dl is:

$$dI\nu = -I_\nu \, n \, \sigma \, dl \tag{4}$$

the solution of this differential equation is easily derived as:

$$I_\nu(l) = I_\nu(0) \, e^{-n\sigma l} \tag{5}$$

Concluding, with ρ the mass density of scatterers and absorbers and κ the opacity of the media, the following relation stands:

$$n \, \sigma = \rho \, \kappa \tag{6}$$

Where $\frac{1}{n \, \sigma}$ is the average distance that the photon travels between interactions.

We will now study the generation and propagation of the photons throughout the dusty media.

2.2 Photon generation and propagation

Having a source S_0 in (x_0, y_0, z_0) we generate N_0 photons γ with initial position $\gamma_0 = (x_0, y_0, z_0)$, zenith angle $\theta_0(-\frac{\pi}{2}, \frac{\pi}{2})$ and azimuth angle $\phi_0(0, \pi)$ (we generate only forward-going photons, that are the ones we are interested in). Supposing L the maximum depth of the dusty media we discretize such length into N steps of size dl.

At each step the probability for a photon to interact along the distance dl is:

$$P_i = n \, \sigma \, dl \tag{7}$$

Therefore for N steps and $dl = L/N$ the probability to travel without any interaction yields to the exponential series:

$$P(L) = (1 - n \, \sigma \, \frac{L}{N})^N = e^{-n\sigma L} = e^{-\tau} \tag{8}$$

Which is just the *pdf* of L and where τ is the *optical depth* along a distance L (number of photons mean free paths along such distance) and it is equal to:

$$\tau = \int_0^L n \, \sigma \, dl \tag{9}$$

The *optical depth* τ is an important and recurrent factor in radiative transfer. It is a measure total transparency and it is very convenient because it unifies the main characteristics of an homogeneous semi-infinite object (depth, density and opacity).

2.3 Scattering and absorbtion

Once the photon has travelled a distance L, if it does still relie on interacting matter (say, it is still inside the dusty area) either scattering or absorbtion will occur. The probability that wether the first or the second phenomenon will

happen depends on the *albedo* of the media. The albedo a is simply defined as the probability for a photon to scatter with respect to the total probability (of scatter and be absorbed):

$$a = \frac{n_s \, \sigma_s}{n_s \, \sigma_s + n_a \, \sigma_a} \tag{10}$$

By setting $a = 1$ we have total scattering while by setting $a = 0$ we have total absorbtion.

2.4 Mean Intensity, Flux and Radiation Pressure

The *mean Intensity* J, the *mean Flux* H and the *mean Radiation Pressure* K are very important astrophysicsl measures. They are also called *intensity moments* and they are used to measure the thermodinamical and mechanical forces acting throughout the dusty media. They are defined as:

$$J = \frac{1}{4\pi} \int I d\Omega \tag{11}$$

$$H = \frac{1}{4\pi} \int I cos(\theta) d\Omega \tag{12}$$

$$K = \frac{1}{4\pi} \int I cos(\theta)^2 d\Omega \tag{13}$$

We have well known theoretical solutions for those values, hence they represent a strong validation measure for the model we have implemented and we therefore will use it to prove it.

See [1] and [2] for more details on radiative transfer theory.

3 The plane parallel slab

3.1 Scenario

We now model the simple case where between the source and the observer there is a plane parallel, uniform, homogeneous and semi-infinite slab of dust. The scenario is depicted in Figure 2.

In this case, the probability for a photon to interact before reaching the slab is zero, hence we neglect the empty space between the light source and the slab and we generate photons isotropically directly from the source-side surface border of the slab.

For sake of simplicity we will assume the slab to have always depth of 1.0 and different configurations of maximum optical depth τ_{max} (so different configuration of ρ and κ).

The density ρ and the opacity κ are considered to be homogenous across the space, we can therefore sample the length that a photon travels from (8) with the inversion method of (14).
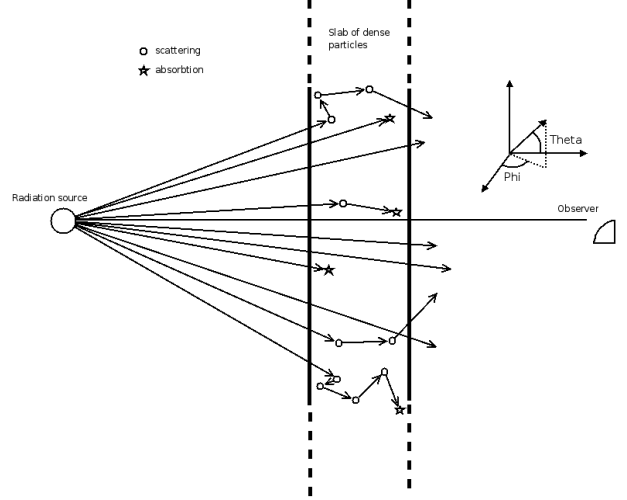

Figure 2. Plane parallel slab

$$l = -\frac{ln(\xi)}{n \, \sigma} \tag{14}$$

With ξ our uniform random number generator in $(0, 1)$. Simplifying, we can parametrize the slab by its total vertical optical depth $\tau_{max} = n \, \sigma z_{max}$ (with z_{max} the total the depth of the slab). We would then sample the optical depth τ as:

$$\tau = -ln(\xi) \tag{15}$$

And we would normalize it to τ_{max} obtaining l with:

$$l = \frac{\tau \, z_{max}}{\tau_{max}} \tag{16}$$

3.2 Isotropic scattering

The simplest scattering technique is the *isotropic scattering*. It consists on having a uniform probability distribution of the scattering angles $\theta \in (0, 2\pi)$ and $\phi \in (0, \pi)$.

This models an ideal case and it cannot represent real dust scattering where, as we will see further, the scattering is not isotropic and it depends on the incident angle of the photon at the moment of the interaction.

3.2.1 Validation

Isotropic scattering is a simple approximation of the reality, nevertheless it is well studied and analytical solutions for some measures of the system are available from the literature.

The most important validation measure is the relation between the incident θ angle of the photons and the normalized total intensity I. The results are shown in Figure 3

where the solid line corresponds to the analytical solution ($Chandrasekhar$ [2] 1960) and the points are the Monte Carlo simulation (see [1], Figure 1a).
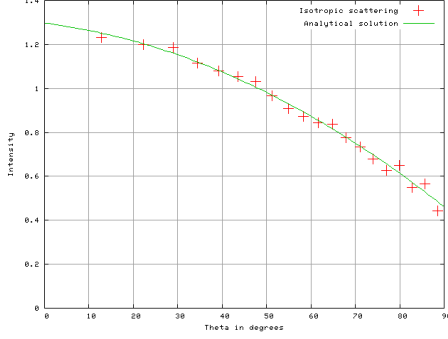

Figure 3. Total intensity I for a plane slab with $\tau_{max} = 10, a = 1$ against the exiting θ angle

As we discussed previously, another strong validation measure are the intensity moments J, H, K. In order to calculate them for a plane parallel structure we divide the slab into *n* parallel slices, orthogonal to the viewing plane. We then compute the moments for each slice and we finally plot the J, H, K values across the slab using the discretized formulae:

$$J = \frac{B_\nu}{4N_0} \sum_i \frac{1}{|\mu_i|} \tag{17}$$

$$H = \frac{B_\nu}{4N_0} \sum_i \frac{\mu_i}{|\mu_i|} \tag{18}$$

$$K = \frac{B_\nu}{4N_0} \sum_i \frac{\mu_i^2}{|\mu_i|} \tag{19}$$

Where B_ν is the *total flux* and N_0 is the total number of photons we generate. The results are shown in Figure 4.

The data we obtained are coherent with [1] (Figure 1b). Once validating the model, we can perform several interesting experiments and measures with it, as described in the following section.
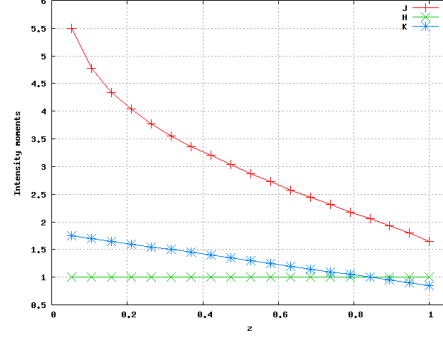

Figure 4. Intensity moments for a plane slab with $\tau_{max} = 10, a = 1$

3.2.2 Results and measures

Using isotropic scattering we can conduct simple but interesting experiments: we generate 10M photons from a point source throught a slab of maximum optical depth $\tau_{max} = 10$. Figures 5, 6 and 7 show the variation of the intensity I for different values of *albedo* (0.6, 0.8, 1.0).
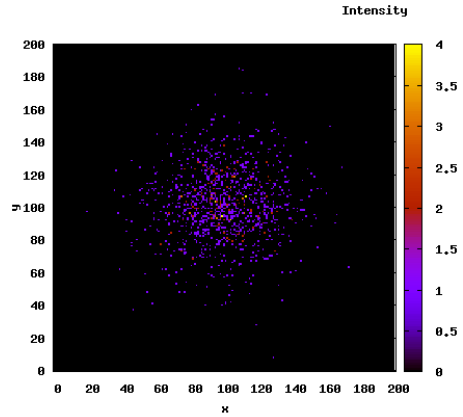

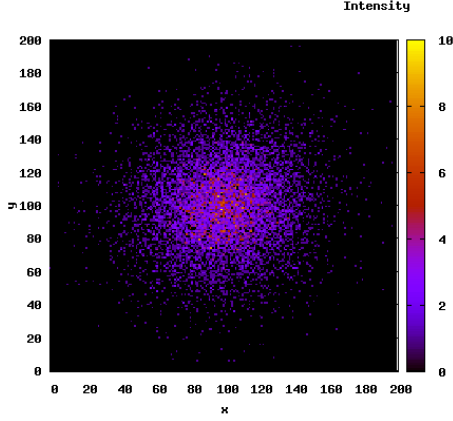**Figure 5.** Intensity for $\tau_{max} = 10$, 10M photons and albedo of 0.6

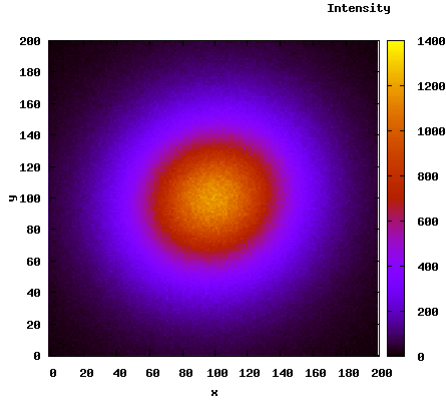**Figure 6.** Intensity for $\tau_{max} = 10$, 10M photons and albedo of 0.8

Figure 7. Intensity for $\tau_{max} = 10$, 10M photons and albedo of 1.0

Figure 8. Total normalized intensity for $\tau_{max} = 10.0$, 1M photons, and variations of albedo

sity ρ (so the optical depth τ). Such relation is expressed by Figure 9.

Figure 9. Intensity values with respect to variations of τ_{max} (1M photons, 1.0 albedo)

The relation between the intensity and the albedo resulted from the simulation is depicted in Figure 8. As it appears from pictures 5, 6, 7 and 8 the intensity that reach the observer seems to increase exponentially with the albedo.

We suppose that is because along a path L_k with k average interactions, the probability to avoid absorption is $(1 - a^k)$ and such polinomial term is increased by the several other factors induced by the scattering process.

From another perspective, linear variations of the media density ρ lead to linear variations of the optical depth τ.

As we sample the non-interaction length L from $-\frac{ln(\xi)}{\rho\kappa}$, we expect L to decrease like ρ^{-1}, decreasing in this way the signal/noise ratio $\frac{S}{N}$.

In particular we found a logarithmic relation between the total intensity I that reaches the observer and the slab den-
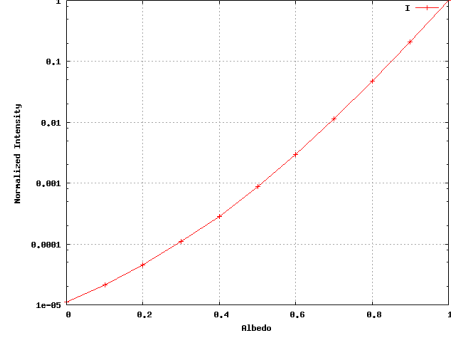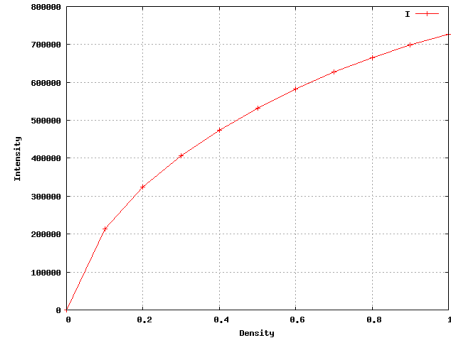
The exiting photons, appropriately projected into the observer's frame are shown in Figures 10, 11, 12 for 10M photons and albedo 1.0.

Using a constant scale as in Figure 13 it is more clearly what it would be visible of the stellar system by an eventual telescope if increasing the optical depth (a denser dust layer).
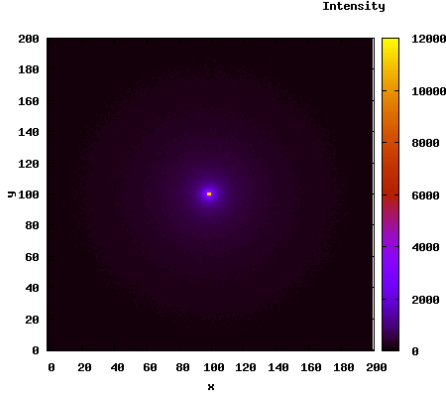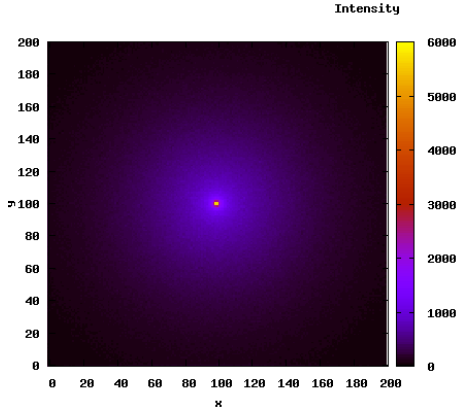
Figure 10. Intensity for $\tau_{max} = 1.0$

Figure 11. Intensity for $\tau_{max} = 2.5$

Figure 12. Intensity for $\tau_{max} = 5.0$
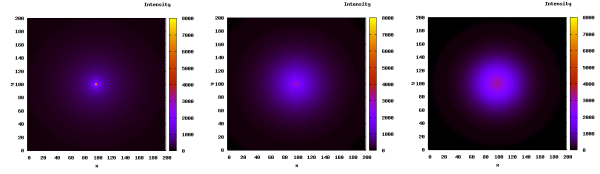
Figure 13. Intensity for $\tau_{max} = 1.0, \tau max = 2.5, \tau_{max} = 5.0$ respectively with constant scale

3.3 Anisotropic scattering: dust

3.3.1 Theoretical background

Isotropic scattering with no polarization is not a good approximation for many problems. Using instead *Rayleigh* scattering and the *Henyey-Greenstein* phase function we are able to approximate dust scattering.

Rayleigh scattering happens when the scattering particles are much smaller than the wavelength of the light crossing them, for example in the Earth's athmosphere (where *Rayleigh* scattering causes the tipical blue colour of the sky) or in our dusty stellar systems.

For anisotropic scattering the new scattering angle is obviously not uniformly distributed, but depends on the incidend angle of the photon at the moment of the interaction and on several others parameters. Moreover the anisotropic scattering algorithm we are using keeps track of the polarization state of each single photon in the system along its path.
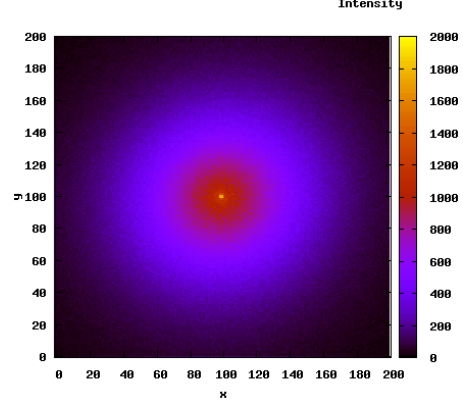
The polarization state of an electromagnetic wave depends on the complex amplitudes E_x, E_y of the electric field E along the two axis, orthogonal to the direction of travel. To define the polarization state space of a photon we use the Stokes' parameters [3] (I, Q, U, V) computed with respect to three vector bases: the standard *Cartesian* basis $(\hat{x}, \hat{y})$, a 45 degrees rotated *Cartesian* basis $(\hat{a}, \hat{b})$ and a circular base $(\hat{l}, \hat{r})$ as follows:

- $I \equiv |E_x|^2 + |E_y|^2$

- $Q = I\rho cos(2\phi)cos(2\theta) \equiv |E_x|^2 - |E_y|^2$

- $U = I\rho sin(2\phi)cos(2\theta) \equiv |E_a|^2 - |E_b|^2$

- $V = I\rho sin(2\theta) \equiv |E_l|^2 - |E_r|^2$

Where *I* is the total intensity, *Q* and *U* are the linear polarizations relative to the standard basis and the rotated basis respectively, *V* is the circular polarization. Note that the 2θ and 2ϕ terms model the fact that the polarization is invariant for rotation of 180'. Figure 14 shows the geometrical meaning of the Stokes' parameters where $(I, Q, U, V) = (S_1, S_2, S_3, S_4)$, while examples of possible polarizations are shown in Figure 15.
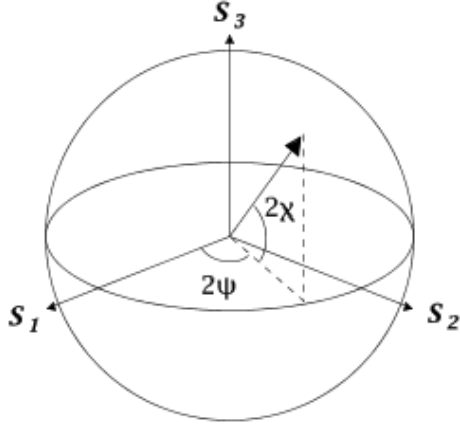
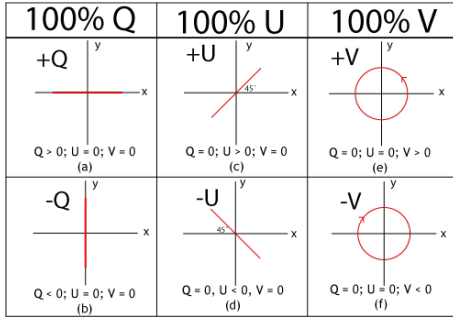**Figure 14.** Poincaré sphere representing the Stokes parameters

Figure 15. Example of possible polarizations using Stokes' parameters

In our simulation the polarization state of each new photon emitted from the source is initialized to $(1, 0, 0, 0)$ which is the case where we have no initial polarization (in absence of magnetic or electric fields). In other words the likelyhood of any polarization state at the photon source is uniform.

Each time a photon scatters its polarization changes and so does its Stokes' vector according to the following equation:

$$S' = L(\pi - i_2)RL(-i_1)S \tag{20}$$

Where the matrix R describes the scattering probability depending on the incident angle of the photon and L is the *Mueller* matrix that rotates towards the coordinates of the observer. In absence of magnetic fields the scattering ma-

trix R is relatively simple:

$$R(\Theta) = a \begin{pmatrix} P_1 & P_2 & 0 & 0 \\ P_2 & P_1 & 0 & 0 \\ 0 & 0 & P_3 & -P_4 \\ 0 & 0 & P_4 & P_3 \end{pmatrix}$$

While the *Mueller* matrix just rotates the system depending on the observer's frame:

$$L(\psi) = a \begin{pmatrix} 1 & 0 & 0 & 1 \\ 0 & cos(2\psi) & sin(2\psi) & 0 \\ 0 & -sin(2\psi) & cos(2\psi) & 0 \\ 0 & 0 & 0 & 1 \end{pmatrix}$$

For dust scattering the matrix R must be filled in with the following values:

$$P_1 = \frac{1 - g^2}{(1 + g^2 - 2g \, cos(\Theta))^{3/2}} \tag{21}$$

$$P_2 = -p_l \, P_1 \frac{1 - cos(\Theta)^2}{1 + cos(\Theta)^2} \tag{22}$$

$$P_3 = P_1 \frac{2cos(\Theta)}{1 + cos(\Theta)^2} \tag{23}$$

$$P_4 = -p_c \, P_1 \frac{1 - cos(\Theta_f)^2}{1 + cos(\Theta_f)^2} \tag{24}$$

Where:

- g is the scattering asimmetry parameter (0 = isotropic scattering, 1 = forward-throwing)

- p_l is the peak linear polarization

- p_c is the peak circular polarization

- $\Theta_f = \Theta(1 + 3.13se^{-7\Theta/\pi})$, with s the skew factor (taken to be unity as described by [5]).

At this point we solve the system 20 as follows:

- we sample i_1 from a uniform angular distribution ($i_1 = 2\pi\xi$)

- we sample Θ from the scattering matrix R as follows:

$$cos(\Theta) = \frac{1 + g^2 - [(1 - g^2)/(1 - g + 2g\xi)]^2}{2g}$$

- we calculate i_2 and the new scattering angles θ and ϕ (see [2] for the details)

- we then compute the new Stokes' parameters S, in this way we can keep track of the polarization state of the photon along its path.

Having the new angles θ and ϕ we can scatter the photon and we step forward to the next interaction.

3.3.2 Validation

Again as we did for the isotropic scattering we need to validate the model. The *Chandrasekhar* analytical solution however refers only to the isotropic case. Hence we set the scattering asimmetry parameter g to 0 in order to simulate isotropic scattering. We then plot the relation between the normalize intensity I and the exiting θ angle of the photons. The results are shown in Figure 16: the solid line is the *Chandrasekhar* analytical solution while the points are our Monte Carlo code.
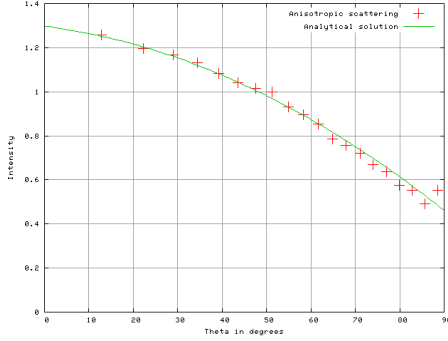

Figure 16. Total intensity I for a plane slab with $\tau_{max} = 10$ against the exiting θ angle

Finallt we again plot the moments J, H and K using the anisotropic scattering algorithm (Figure 17).
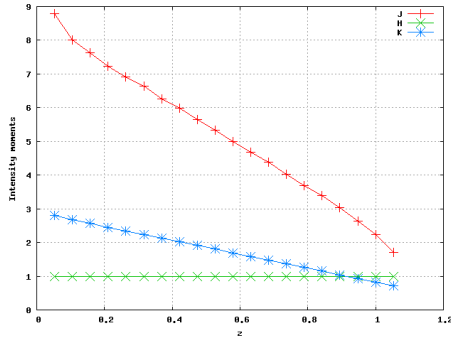

Figure 17. Intensity moments using anisotropic scattering for the *ultraviolet* band and density $\rho = 0.01$ but with $g = 0$ (see table at 3.3.3)

3.3.3 Results and measures

The properties of interstellar dust (total opacity, albedo, scattering asimmetry parameter and peak linear polarization) are well known and they are available in literature for many radiation bands. Those values, together with the described scattering technique permit us to do very interesting expriments. We simulate a parallel slab with depth 5.0 assuming also constant density of 0.001 and changing the total opacity κ according to the following table.

Band $\lambda(\mu m)$	κ	a	g	p_l
U(0.34)	360	0.54	0.48	0.26
B(0.44)	286	0.54	0.48	0.31
V(0.55)	219	0.54	0.44	0.43
R(0.73)	156	0.53	0.37	0.58
I(0.85)	105	0.49	0.29	0.70
J(1.25)	65	0.43	0.16	0.75
H(1.65)	38	0.33	0.06	0.87
K(2.20)	20	0.21	0.02	0.93

The results in Figures 18 and 19 show how the same stellar system, simulated with 100M photons, appears if seen either through the *ultraviolet* band U or through the *infrared* band K (see 3.3.3).
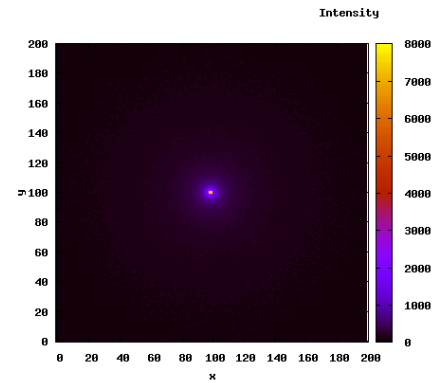

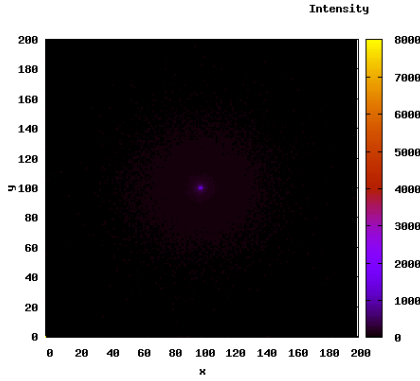**Figure 18.** Intensity for the ultraviolet band U

Figure 19. Intensity for the infrared band K

Although the ultravioled band has a higher total opacity, the albedo is more than a half of the albedo of the infrared band. Moreover the scattering in the infrared is almost isotropic while the asimmetry parameter for the ultravioled band is 24 times larger.

4   3-dimentional cartesian grid

4.1   Basic concepts

In order to simulate a variety of dust clouds around a point source it is necessary to discretize the space. In this way, clouds of different densities and shape can be created, where every cell contributes differently to the optical depth. The space is discretized in each direction to $xdim \cdot ydim \cdot zdim$ grid cells and $(xdim + 1) \cdot (ydim + 1) \cdot (zdim + 1)$ cell faces where each cell has a defined opacity value $\rho_{x,y,z}$.

Therefore, we can no longer aproximate the $n\sigma$ term to a constant value as for the plane parallel slab. Each time we generate or we scatter a photon we must instead compute the integral of the opacity along its path until the edges of our grid as explained by 9. We will use such value to sample the new L as in 14. With such grid we can just decide which kind of configuration of interacting media we want and simulate its distortion effect on a light source.

4.2   Integration

The integration technique used to calculate the randomly sampled optical depth of each run τ traces the course of the photon through the grid. For each cell face that the photon crosses (in x, y or z direction) the corresponding contribution of this cell to the total τ travelled is computed. This means that the contribution of the cell crossed to the total τ

of the particular run is the actual distance travelled through the cell multiplied by the cell's density.

The distance to the next cell faces along the propagation unit vector (n_x, n_y, n_z) is calculated using:

$$s_x = \frac{xface - x}{n_x}, s_y = \frac{yface - y}{n_y}, s_z = \frac{zface - z}{n_z} \tag{25}$$

It is reasonable that the photon will hit the minimum of these distances first. The integration process is over when $\tau_{run} + \tau_{cell} > \tau$. When this happens, the photon scatters into the cell at a distance

$$s = \frac{(\tau - \tau_{run})}{\rho_{cell}} \tag{26}$$

4.3   Results and experiments

The first experiment we conducted is the simulation of a uniform and homogeneous cube of dust of dimensions (x, y, z) placed in front of the source at position (x, y, z) as shown in Figure 20.
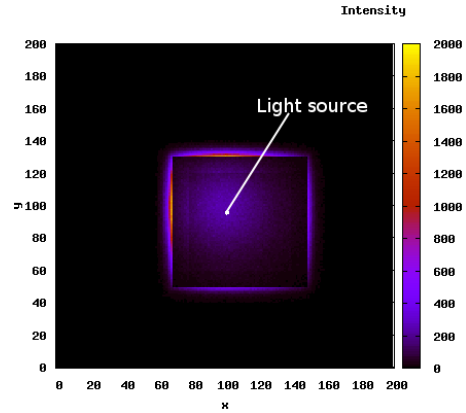

Figure 20. Intensity for a cube of dust placed in front of the source

The asymmetrical position of the cube permits to notice clearly the boundary effects. Along the borders in fact a very large number of photons is projected from the side planes of the cube towards the observer, producing high dencity spots. Also the backside boundaries of the cube are visible from the perspective.

Another interesting experiment we performed consisted on simulating the case where we have a star in the middle of an oblate spheroid described by

$$x^2 + \frac{y^2}{c} + z^2 = r \tag{27}$$

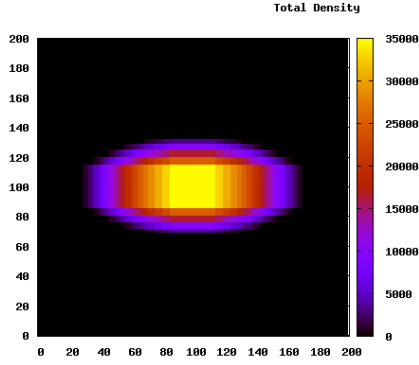with $c = 5$ and where the density ρ is depicted in Figure 21.

Figure 21. Density distribution of an oblate spheroid of dust with a point source in the centre
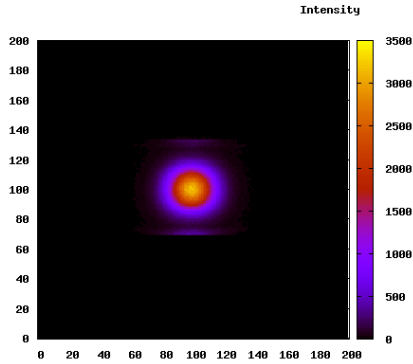
The results we obtained are shown in Figure 22.

Figure 22. Intensity of a spheroid dusty cloud using 2M photons, a=1.0 and density distribution of Figure **??**

As it can be seen, still we notice the boundaries of the structure. It is however interesting to study the influence of the distribution of density in the final image.

Concluding, the cartesian grid offers a simple and clean method to simulate complex shapes of dusty material but at the same time needs a huge amount of memory (we could simulate up to 200x200x200 of grid points).

5 Parallelization

One of the best options when parallelizing a Monte Carlo simulation is the task farming approach, that is using a number of machines to draw different samples from the parameter space. This is possible as we assume that the sampling events in the Markov chain created are themselves independent of all the previous sampling events. Also, since in most cases the complexity of the spatial domain does not exceed the processing capabilities of the individual machines, complex domain decomposition schemes would only add unneeded overhead to the simulation.

In the case of the radiative transfer code, the independence of the events in the Markov chain allows us to distribute the burden of the simulation to the available processors by assigning a subset of the number of photons to each processor. Then, the simulation domain is initialized on each processor using the parameters broadcasted from the root node. Since there is no spatial decomposition, the simulation proceeds independently on each processor with minimal communication overhead. There is then only one global communication step at the end of the simulation when we compute the global reduction of the individual simulation results from all processes to the root process.

The code is written in C++, which makes it reasonably portable and fast compared to other languages. The parallelization is achieved using functions from the robust MPI library, which is the standard choice for clustering computation. All of the results have been obtained using the OW cluster of the UvA.

5.1 Results

Given the high level of scalability of the radiation transfer problem and therefore the small communication overhead it introduces we expect a quasi-linear speedup. The efficiency of the parallelized code is shown on Figure 23. The results are very satisfactory, the speedup is almost linear and permits to fully gain computational power from a cluster of machines as we did in almost all the discussed experiments.
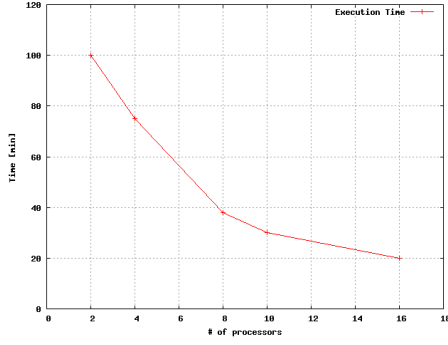
Figure 23. Parallelization efficiency (OW cluster at UvA)

6   Conclusion

The radiation transfer problem is a crucial issue when we want to model many astrophysical systems and Monte Carlo methods are particularty suitable for this kind of problem. In this paper we have investigated how we can use Monte Carlo techniques in order to model radiative transfer in dusty stellar systems. We gave a brief theoretical background and we studied and implemented the different scattering techniques. We discussed the solution of the cartesian grid for modeling inhomogeneous media and we finally presented a distributed version of our code.

References

[1] K. Wood, B. Whitney, J. Bjorkman, M. Wolff, *Introduction to Monte Carlo radiation transfer*, September 27, 2001. 2.4, 3.2.1, 3.2.1

[2] S. Chandrasekhar, *Radiative transfer*, Dover Publication, 1960. 2.4, 3.2.1, 3.3.1

[3] H. C. van de Hulst, *Light scattering by small particles*, Dover Publications, New York, 1981, p42. 3.3.1

[4] N. Metropolis, *The beginning of the Monte Carlo method*, Los Alamos Science Special Issue, 1987. 1.1

[5] M. G. White, S. H. Southworth, P. Kobrin, E. D. Poliakoff, R. A. Rosenberg and D. A. Shirley, *Angular distribution of Xe $5s \rightarrow \epsilon p$ photoelectrons near the Cooper Minimum*, Physics Review Letters, 26th November 1979. 3.3.1